

Mid-Infrared Micro-Displacement Measurement with a Bidimensional Silicon Photonic Crystal

Tarek Zouache* and Abdesselam Hocini

Abstract—In this work, a micro displacement sensor based on dual micro-cavities coupled to a photonic crystal waveguide is proposed. The defects are introduced to create a sharp resonance in the structure which makes it useful for detecting micro displacement changes. The sensing principle is based on the change of the output signal transmission with the change of the displacement of a moving part compared to a fixed part of sensor structure. The proposed structure reached a good sensitivity of $9.52a^{-1}$.

1. INTRODUCTION

Photonic crystals (PhCs) are artificial periodic structures with a material whose dielectric permittivity is modulated periodically on one, two, or three directions in space [1]. This periodic variation produces a forbidden wavelength region called photonic band gap (PBG) which prohibits the propagation of light in the material because of the existence of the permitted optical modes propagation in this region. Such structures are made exploitable by introducing certain defects such as point defects as cavities or line defects as waveguides, and their coupled elements in the structure can adjust the dispersion diagram hence permit particular modes to propagate in the bandgap [2]. The light confinement and control offered by PhCs can be used to enhance the performance and reduce the size of many important optical components, such as lasers, semiconductor optical amplifiers [3–5]. More of that, the interaction between a cavity resonator and a waveguide has been previously used in tremendous research works in different fields such as displacement measurement and sensing [6–9]. The latter application has always been very important in engineering. Of course, for many applications, the measurement and control of micro-displacement have a great importance for their good functioning, such as aerospace, health control devices (scanner and medical imaging), and micro-electromechanical systems (NEMS). This kind of sensor is a key element in measurement and also for the precise control of microscopic displacement. Consequently, it is potentially important for applications such as atomic force microscopy (AFM) and biochemical detection [10–12]. The first ultra-sensitive designs were proposed by Levy et al. [6] for displacement detection used photonic crystal waveguides. Levy et al. have demonstrated that such devices could provide sensitivity close to $1.0\ \mu\text{m}^{-1}$ with a light source of $9.02\ \mu\text{m}$. Then, Xu et al. [7] presented a micro-displacement sensor using a disconnected two-dimensional photonic crystal (the material used had refractive index of 3.4) with square lattice and a linear resonant cavity defect. This sensor could measure the displacement in a range of $-0.55a$ to $0.60a$. For the study of the behavior of this sensor, this range was segmented into 6 sub-ranges with each range having its own wavelength excitation. The best sensitivities obtained by these two authors were $1.90a^{-1}$ for the range $-0.55a-0.4a$ (the normalized working frequency is 0.343) and $1.62a^{-1}$ for the displacement range of $-0.4a-0.2a$ (the frequency normalized workload is 0.341). In 2011, Yang et al. [8] provided a sensor consisting of a connected two-dimensional silicon slab with a triangular network of air holes. This silicon substrate contained a slot and a micro-cavity made by removing a single hole. The two horizontal holes adjacent

Received 8 April 2020, Accepted 6 May 2020, Scheduled 22 May 2020

* Corresponding author: Tarek Zouache (tarek.zouache@univ-msila.dz).

The authors are with the Laboratory Analyse de Signaux et de Systemes, Department of Electronics, Faculty of Technology, University of Msila, Algeria.

to the micro-cavity would be displaced by an amount Sx along the $+X$ and $-X$ axes respectively to control the micro-cavity transmission and its sensitivity. This sensor was composed of two segments, a fixed left segment and a mobile right segment. By choosing a suitable normalized excitation frequency $\omega_0 = 0.2492(2\pi c/a)$ and for $Sx = 0.2a$, Yang et al. acquired a linear sensor response with a sensitivity of $1.0a^{-1}$ and a cavity quality factor Q of 6000 in the displacement range of $0.0a$ to $0.20a$. In 2014, Olyee and Azizi [9] provided a high sensitivity sensor. This sensor was made with a 3.4 refractive index material and an air holes matrix in a square network. By choosing a wavelength of $2.7 \mu\text{m}$, the sensitivity that they could reach was $3.6 \mu\text{m}^{-1}$ – $3.8 \mu\text{m}^{-1}$ according to the radius of the holes chosen (by choosing a radius of holes between $0.49 \mu\text{m}$ and $0.51 \mu\text{m}$, sensitivity and regression have optimal values) with a quality factor close to 180. The linearity of this sensor has been obtained in the range of $0.0 \mu\text{m}$ to $0.5 \mu\text{m}$.

2. SENSOR DESIGN

The structure adopted for the displacement sensor uses a triangular network consisting of a 23×21 air holes matrix with a radius r formed in a silicon substrate ($r = 0.33a$, and a is the period of the photonic crystal). The refractive index of silicon is $n_{\text{Si}} = 3.48$ [7], and the thickness of the slab is $h = 490 \text{ nm}$. This slab is deposited on a SiO_2 layer with a refractive index of 1.45 [7], and a thickness h_{SiO_2} is of $1.5 \mu\text{m}$. The incident source is a Gaussian pulse with a wavelength of $3.6 \mu\text{m}$. While most silicon-based photonic components have been generally made in near infrared telecommunication band, the mid-infrared band (average IR: wavelength range 2 – $20 \mu\text{m}$) also offers a great and significant opportunity for the growth of integrated photonics. There are now various key devices based on silicon using this wavelength band, such as waveguides, light sources, modulators, and detectors. Integrated photonic devices are also capable of providing containment optical at the sub-wavelength scale which considerably increases the light-matter interaction as well as the signal-to-noise ratio (SNR) [13–15]. The calculation of the silicon effective refractive index (n_{eff}) gives the value of 2.654. The use of effective index gives a good approximation of the 3D model simulation and reduces the simulation time considerably [16, 17].

Figure 1 illustrates the normalized frequency dispersion pattern with respect to the wave vector of the original photonic crystal matrix.

Without defects, the initial structure has a wide band gap between $3.0001 \mu\text{m}$ and $3.9550 \mu\text{m}$ and centered at $3.4775 \mu\text{m}$ for the TM polarization only in the Γ -K-M- Γ directions of the Brillouin zone (see Fig. 1). This band gap corresponding to TM polarization will be used in the following as the sensor's operating range. This result is obtained using the two-dimensional PWE method integrated into the RSoft Band Solve software.

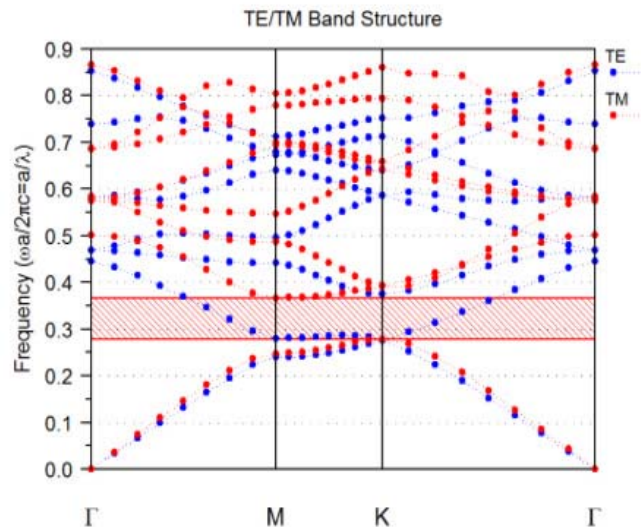


Figure 1. Photonic band gap of the designed sensor.

3. PRINCIPLE OF DETECTION AND SIMULATION

3.1. Principe of Detection

The change of the distance between the mobile and the fixed parts of the sensor will change the transmission of the output optical signal. As a result and in the case where the sensor parameters are properly optimized, it must be a displacement range in which the transfer function of the sensor (the relation between the displacement input and the output transmission) will be linear. At an appropriate operating frequency, the proposed structure can be used as a micro displacement sensor with high sensitivity. The transmission coefficients for different frequencies can be expressed approximately by the following Lorentz function given in Eq. (1) [8, 9]:

$$T(\omega_0, \omega_1) = \frac{\frac{\omega_0}{2 \times Q}}{(\omega_0 - \omega_1)^2 + \frac{\omega_0}{2 \times Q}} \quad (1)$$

ω_0 is the resonance frequency, and Q is the quality factor of the resonant cavity of the structure. When the moving segment is shifted along the axis of displacement with an operating frequency ω_0 , we can then deduce the variation of the transmission coefficient Δx as given in Eq. (2). Using a serial development of Taylor, we will have [8, 9]:

$$\Delta T(\Delta x) = T(x + \Delta x) - T(x) = T(x)' \times \Delta x + \frac{T(x)''}{2} \times \Delta x^2 + O(\Delta x) \quad (2)$$

Δx is the distance between the two segments.

Generally and in practice, when designing this kind of sensor, we must find a pulsation ω_1 (or a wavelength λ_1) that ensures its linear operation within the displacement range [7]. Once this wavelength is defined, the relation in Eq. (2) becomes linear, which implies that [6]:

$$T(\omega_0, \omega_1)'' \approx 0, \quad \Delta T(\Delta x) = T(x)' \times \Delta(x) \quad (3)$$

Then and finally, the sensitivity of this sensor is given by Eq. (4) [6]:

$$S = \frac{\Delta T(\Delta x)}{\Delta x} \quad (4)$$

3.2. The Sensor Simulation

The design of our displacement sensor consists of two parts, one fixed (left part) and the other movable (right part). The two parts are located on either side of the central axis OZ slab. The moving step of moving part is a fraction of the period a . In our calculations, this step and the total displacement range will be taken $0.05a$ and 0 to $0.2a$, respectively; this range is used in several existing works in the literature [8, 9]. In the basic structure, a central waveguide and two H_0 cavities are made on either side of the OX and OZ axes as shown in Fig. 2(a).

Both the H_0 micro-cavities are obtained by shifting the yellow holes with $Sx = 0.335D$ shift (D is the distance between two adjacent holes) in the two opposite directions $+OX$ and $-OX$ at the same time. The value $0.335D$ of Sx is obtained after several optimization processes. These processes consist in that the first time change Sx by steps of $0.1D$ between 0 and $0.8D$. Then this process is repeated for a second time by changing Sx by a step of $0.01D$ and later for a third time by varying Sx by steps of $0.001D$ end at the end of each optimization step, and we choose the value of Sx offering the best sensitivities. Finally, we obtain $Sx = 0.335D$ as the final optimal values. To enhance the sensitivity of the obtained sensor we have used a second shift process with concern the purple holes as indicated in Fig. 2(b). The shift value Sy is $0.05D$ which is determined by using an optimization process similar to the one used below. The useful part of the output spectrum is shown in Fig. 3.

The light excitation used in this simulation is a laser of wavelength $= 3.6 \mu\text{m}$ with a Gaussian distribution, and the simulations realized using the finite-difference time-domain (FDTD) algorithm [18] and the plane wave expansion (PWE) method integrated in the FullWave component of the RSoft software.

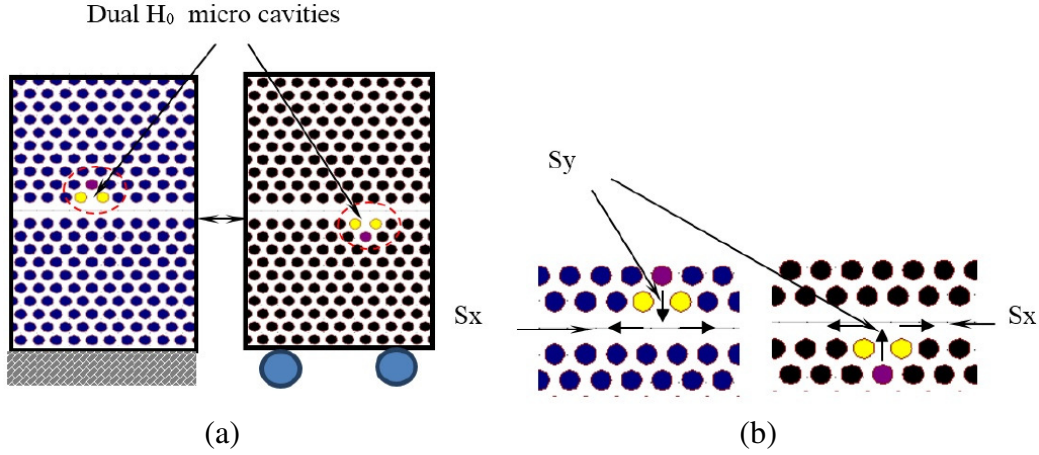


Figure 2. (a) Proposed design for the micro displacement sensor, (b) optimizations process.

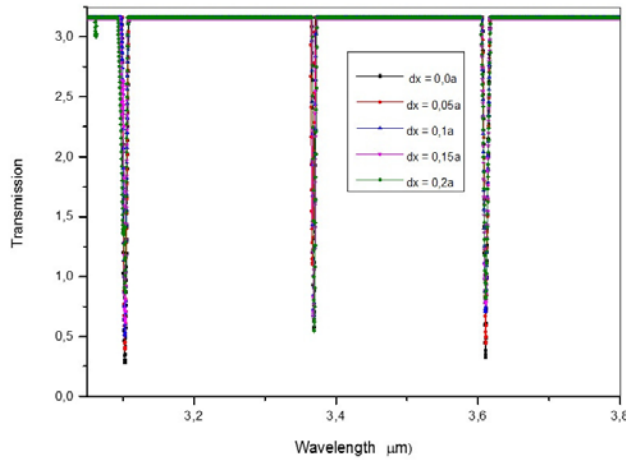


Figure 3. Response of the micro displacement sensor as a function of wavelength for various displacements Δx (dx in Figure 3).

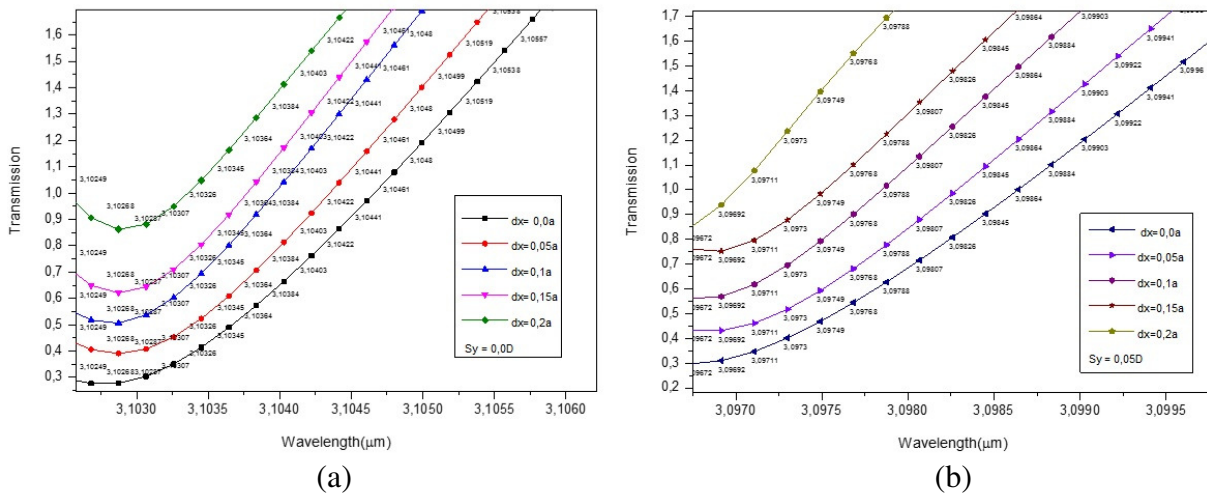


Figure 4. Sensor response for various displacements with $S_x = 0.335D$ and: (a) For $S_y = 0$ and (b) for $S_y = 0.05D$.

For both cases of Sy ($Sy = 0.0D$ and $Sy = 0.05D$), the sensor response spectrum shows three groups of pulses. In the following study, we want to consider only the first pulses groups, because of it gives better characteristics for our sensor. The pulses groups are located around the wavelength $3.1178 \mu\text{m}$ (for $Sy = 0$) and a second one with a central wavelength close to $3.0967 \mu\text{m}$ (for $Sy = 0.05D$). Fig. 4(a) and Fig. 4(b) give a zoom of the first pulses groups respectively for $Sy = 0$ and $Sy = 0.05D$. Each region, as we can see, can be divided in several operating regions where every region is defined for an explicit wavelength as shown in both figures. The spectrum of Fig. 5 is the same as that of Fig. 4, except that the spectrum in Fig. 5 gives the transmissions with respect to the maximum of the spectrum, which is $3.1630(\text{AU})$ and not to transmission origin (Transmission equal to zero).

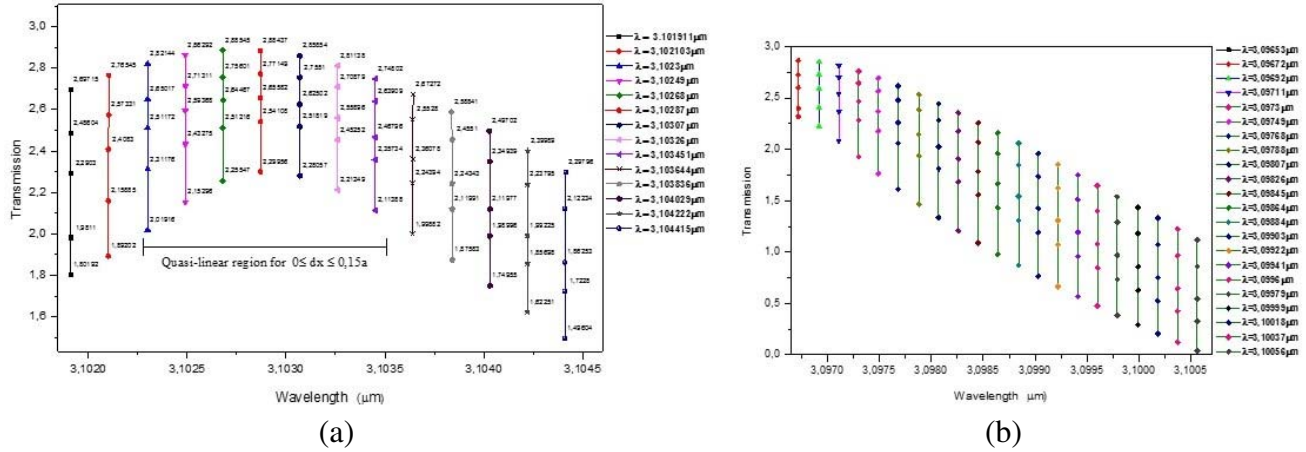


Figure 5. Sensor output spectrum for various displacements with $Sx = 0.335D$ and, (a) for $Sy = 0$, (b) for $Sy = 0.05D$.

3.3. The Sensor Sensitivity

The sensitivity is defined according to Eq. (4), and it is more important when the proposed structure provides a large output transmission difference for a small moving distance Δx . The sensitivity is calculated from Eq. (4). The results are gathered in Table 1.

4. RESULT AND DISCUSSIONS

Table 1 gives the best sensitivity reached by our proposed structure. We can see that for $Sy = 0$ and wavelength λ between $3.10268 \mu\text{m} \leq 3.10307 \mu\text{m}$, the sensibility is quasi-constant for a displacement range from 0 to $0.15a$. A high sensitivity of $5.14a^{-1}$ is also reached for $\lambda = 3.10268 \mu\text{m}$. Now for the second case where $Sy = 0.05D$, the sensitivity is not constant over the whole range of displacement $0.0a$ to $0.2a$, but variable depending on the considered displacement distance of the mobile part. We can deduce that after applying the shift $Sy = 0.05D$, we have seen a very significant improvement in sensitivity. Effectively as can be seen in the corresponding part of Table 1, for all wavelengths of the new obtained transmission spectrum (for the lengths of waves greater than $3.09788 \mu\text{m}$) and also for all the sensor displacement intervals, the new obtained sensitivity is between $3.0a^{-1}$ (for 3.09788 and a displacement between 0 and $0.05a$) and $9.52a^{-1}$ (for $3.09807 \mu\text{m}$ and a displacement between $0.15a$ and $0.2a$). Table 2 provides a comparison between our results and others obtained by other authors.

Comparing our results to others found in literature, we can say that ours are very acceptable in most cases, and we have also reached a maximum of $9.52a^{-1}$ which is very important compared to works done by other authors.

Table 1. Calculated sensitivity as a function of wavelength λ , (a) for $Sy = 0.0$, (b) for $Sy = 0.05D$.

(a)

$\Delta x(a)$	0.0–0.05	0.05–0.1	0.1–0.15	0.15–0.2
λ (μm)	Sensitivity (a^{-1}) for $Sy = 0.0D$			
3.10268	2.56	2.23	2.65	5.14
3.10287	2.26	2.32	2.3	4.83
3.10307	2.07	2.6	2.14	4.75
3.10384	2.67	4.23	2.47	4.9
3.10403	2.95	4.6	2.60	4.81

(b)

$\Delta x(a)$	0.0–0.05	0.05–0.1	0.1–0.15	0.15–0.2
λ (μm)	Sensitivity (a^{-1}) for $Sy = 0.05D$			
3.09788	3.00	4.8	4.18	9.38
3.09807	3.3	5.10	4.34	9.52
3.09826	3.55	5.4	4.47	9.48
3.09845	3.81	5.64	4.58	9.32
3.09864	4.05	5.86	4.65	9.08
3.09884	4.27	6.03	4.70	8.8
3.09903	4.46	6.18	4.73	8.46
3.09922	4.63	6.3	4.73	8.12

Table 2. Comparison of our results and those found in the field literature.

Author	Year	Sensitivity (a^{-1})	Sensitivity (μm^{-1})
Z. Xu et al. [7]	2006	1.15	-
D. Yang et al. [8]	2011	1.0	-
S. Olyee et al. [9]	2014	-	3.6–3.8
Our results		9.52	

5. CONCLUSION

A transmission variation sensing platform for micro displacement detection based on dual micro-cavities coupled photonic crystal waveguide is proposed. The analysis is performed on different values displacement using FDTD method. The variation of transmission caused by the moving part of the sensor compared to a fixed part is detected by measuring the transmission change spectra of the proposed dual micro-cavities coupled with photonic crystal waveguide. Efficient optimization process of the structure has been conducted leading to high sensitivity. The optimization is done by varying both the shifts Sx and Sy of the dual micro-cavities. Consequently, our proposed design shows good displacement sensitivity, and we have reached a very good sensitivity of $9.52a^{-1}$ using this design.

REFERENCES

1. Jouannopoulos, J. D., S. G. Johnson, J. N. Winn, and R. D. Meade, *Photonic Crystals: Molding the Flow of Light*, Princeton University Press, Princeton, NJ, 1995.
2. Goyal, A. K., H. S. Duttaa, and S. Pal, "Recent advances and progress in photonic crystal based gas sensors," *Journal of Physics D: Applied Physics*, Vol. 50, No. 20, 203001, 2017, <https://doi.org/10.1088/1361-6463/aa68d3>.

3. Cao, T., Y.-L. D. Ho, P. J. Heard, L. P. Barry, A. E. Kelly, and M. J. Cryan, "Fabrication and measurement of a photonic crystal waveguide integrated with a semiconductor optical amplifier," *Journal of the Optical Society of America B*, Vol. 26, No. 4, 768–777, April 2009.
4. Cao, T., M. J. Cryan, Y.-L. D. Ho, I. J. Craddock, and C. J. Railton, "Fast-light based pulse compression in 2-D photonic crystal waveguides," *Journal of Lightwave Technology*, Vol. 25, No. 9, 2590–2598, September 2007.
5. Cao, T., M. J. Cryan, P. S. Ivanov, D. Ho, B. Ren, I. J. Craddock, J. M. Rorison, and C. J. Railton, "Modeling of chirped pulse propagation through a mini-stop band in a two-dimensional photonic crystal waveguide," *Journal of the Optical Society of America B*, Vol. 24, No. 7, 1575–1583, July 2007.
6. Levy, O., B. Z. Steinberg, M. Nathan, and A. Boag, "Ultrasensitive displacement sensing using photonic crystal waveguides," *Applied Physics Letters*, Vol. 86, No. 10, 104102–104104, 2005.
7. Xu, Z., L. Cao, C. Gu, Q. He, and G. Jin, "Micro-displacement sensor based on line-defect resonant cavity in photonic crystal," *Optics Express*, Vol. 14, No. 1, 298–305, 2006.
8. Yang, D., H. Tian, and Y. Ji, "Microdisplacement sensor based on high-Q nanocavity in slot photonic crystal," *Optical Engineering*, Vol. 50, No. 5, 054402, May 2011.
9. Olyaei, S. and M. Azizi, "Micro-displacement sensor based on high sensitivity photonic crystal," *Photonic Sensors*, Vol. 4, No. 3, 220–224, 2014.
10. De Vlaminck, I., J. Roels, D. Taillaert, D. van Thourhout, R. Baets, L. Lagae, and G. Borghs, "Detection of nanomechanical motion by evanescent light wave coupling," *Applied Physics Letters*, Vol. 90, 233116, 2007.
11. Lee, C. and J. Thillaigovindan, "Optical nano mechanical sensor using a silicon photonic crystal cantilever embedded with a nanocavity resonator," *Applied Optics*, Vol. 48, 1797–1803, 2009.
12. Lee, C., R. Radhakrishnan, C. C. Chen, J. Li, J. Thillaigovindan, and N. Balasubramanian, "Design and modeling of a nano mechanical Sensor using silicon photonic crystals," *Journal of Light Wave Technology*, Vol. 26, 839–846, 2008.
13. Lin, H., Z. Luo, T. Gu, L. C. Kimerling, W. Kazumi, A. Agarwal, and J. Hu, "Mid-infrared integrated photonics on silicon: A perspective," *Nanophotonics*, Vol. 7, No. 2, 393–420, 2018.
14. Cao, T., L. Fang, Y. Cao, N. Li, Z. Fan, and Z. Tao, "Dynamically reconfigurable topological edge state in phase change photonic crystals," *Elsevier Science Bulletin*, Vol. 64, 814–822, 2019.
15. Tyoub, H., A. Hocin, and A. Harhouz, "Mid-infrared refractive index sensor based on 2D photonic crystal coupled cavity-two waveguides," *Instrumentation Measure Metrologie*, Vol. 18, No. 2, 165–169, 2019.
16. Qiu, M., "Effective index method for heterostructure-slab-waveguide-based two dimensional photonic crystal," *Appl. Phys. Lett.*, Vol. 81, 1163, 2002.
17. Zouache, T., A. Hocini, and X. Wang, "Cavity-coupled photonic crystal waveguide as highly sensitive platform for pressure sensing," *Optik — International Journal for Light and Electron Optics*, Vol. 172, 97–106, 2018.
18. Ho, D. Y. L., T. Cao, S. Pavel, M. J. I. Cryan, I. J. Craddock, C. J. Railton, and J. G. Rarity, "Three-dimensional FDTD simulation of micro-pillar microcavity geometries suitable for efficient single-photon sources," *IEEE J. Quantum Electronics (JQE)*, Vol. 43, 462, 2007.